Higher-order correlation on polarization beats in Markovian stochastic fields

Yanpeng Zhang*
Department of Electronic Science and Technology, Xi'an Jiaotong University, Xi'an 710049, China

Cid B. de Araújo
Departamento de Física, Universidade Federal de Pernambuco, 50670-901 Recife, Brazil

Edward E. Eyler
Department of Physics, University of Connecticut, U-3046; Storrs, Connecticut 06269
(Received 2 August 2000; published 6 March 2001)

The correlation effects of sixth order on cascade three-level polarization beats are investigated using chaotic field, phase-diffusion, and Gaussian-amplitude models. The polarization beat signal is shown to be particularly sensitive to the statistical properties of the Markovian stochastic light fields with arbitrary bandwidth. Different stochastic models of the laser field only affect the sixth- and fourth-order coherence functions. The constant background of the beat signal originates from the amplitude fluctuation of the Markovian stochastic fields. The Gaussian-amplitude field shows fluctuations larger than the chaotic field, which again exhibits fluctuations much larger than for the phase-diffusion field with pure phase fluctuations caused by spontaneous emission. The cases that the pump beams have either narrowband or broadband linewidth are considered and it has been found that for both cases a Doppler-free precision in the measurement of the energy-level difference of the excited states can be achieved. The sixth-order coherence function theory is of vital importance in cascade three-level polarization beats.

DOI: 10.1103/PhysRevA.63.043802 PACS number(s): 42.65.Re, 42.65.Hw, 32.90.+a

I. INTRODUCTION

The statistical properties of the noisy light field are of particular importance for nonlinear optical processes since these are often sensitive to higher-order correlations in the field. The effects of such correlations have been studied in several nonlinear processes characterized by either Markovian or non-Markovian fluctuations [1–5]. The Markovian field is now described statistically in terms of the marginal and the conditional probability densities [6,7]. The atomic response to non-Markovian fields is much less well understood [4]. This is primarily because the complete hierarchy of conditional probabilities must be known in order to describe a non-Markovian process. Some non-Markovian processes can be made Markovian by extension to higher dimensions.

The atomic response to Markovian stochastic optical fields is now largely well understood [1–3,5]. When the laser field is sufficiently intense that many photon interactions occur, the laser spectral bandwidth or spectral shape, obtained from the second-order correlation function, is inadequate to characterize the field. Rather than using higher-order correlation functions explicitly, three different Markovian fields are considered: (a) the chaotic field, (b) the phase-diffusion field, and (c) the Gaussian-amplitude field. The chaotic field undergoes both amplitude and phase fluctuations and corresponds to a multimode laser field with a large number of uncorrelated modes, or a single-mode laser emitting light below threshold. Since a chaotic field does not possess any intensity stabilization mechanism, the field can take on any value in a two-dimensional region of the complex plane centered about the origin [5]. The phase-diffusion field undergoes only phase fluctuations and corresponds to an intensity-stabilized single-mode laser field. The phase of the laser field, however, has no natural stabilizing mechanism [5]. The Gaussian-amplitude field undergoes only amplitude fluctuations. Although pure amplitude fluctuations cannot be produced by a nonadiabatic process, we do consider the Gaussian-amplitude field for two reasons. First, because it allows us to isolate those effects due solely to amplitude fluctuations and second, because it is an example of a field that undergoes stronger amplitude (intensity) fluctuations than a chaotic field. By comparing the results for the chaotic and the Gaussian-amplitude fields we can determine the effect of increasing amplitude fluctuations [6,7].

This paper addresses the role of noise in the incident fields on the nature of the wave-mixing signal—particularly in the time domain. This important topic has been already treated extensively in the literature including the introduction of a new diagrammatic technique (called factorized time correlator diagrams) [8–14]. They have treated the higher-order noise correlators when circular Gaussian statistics apply. There should be two classes of such two component beams. In one class the components are derived from separate lasers and their mixed (cross) correlators should vanish. In the second case the two components are derived from a single laser source whose spectral output is doubly peaked. This can be created from a single dye laser in which two different dyes in solution together are amplified. The present paper deals only with the first class. That is to say, we are considering only the class of two-color beams in which each color is derived from a separate laser source. In any case the literature has already explored, both theoretically and experimentally, the

*FAX: +86-29-3237910, Email address: yp.zhang@263.net

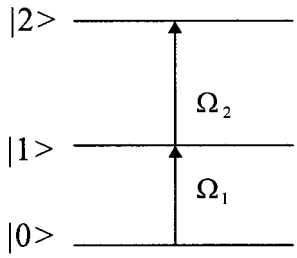

FIG. 1. Cascade three-level configuration to be treated by HOCPB.

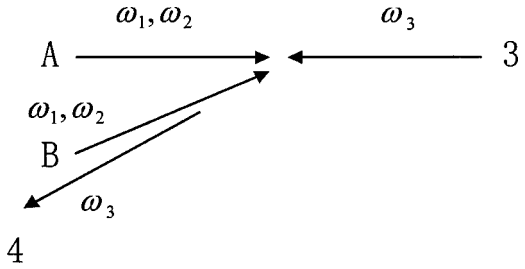

FIG. 2. Schematic diagram of the geometry of HOCPB.

use of such multicolor noisy light in four-wave mixing (FWM) [9,10]. Interestingly, that work only treats the second class of multicolored beams (a single laser source for the multipeaked ''tailored'' light) in self-diffraction geometry. Also that work does not treat the cascade three-level system with phase-conjugation geometry using three types of noisy models, and furthermore its beam 3 is not noisy (it was ''monochromatic'') [9,10].

The chaotic field, the Brownian-motion phase-diffusion field, and the Gaussian-amplitude field are considered in parallel with a discussion on cascade three-level atom transitions. Cascade three level is an accepted nickname for a three-level system in which one color matches the $|0\rangle$–$|1\rangle$ energy gap, the second color the $|1\rangle$–$|2\rangle$ energy gap (Fig. 1). This is different from the ''cascade processes'' in nonlinear spectroscopies, which often refer to the buildup of higher-order polarizations from two (or more) sequential lower-order processes occurring on different spatially separated centers [11]. We develop a unified theory that involves sixth-order coherence function to study the influence of partial-coherence properties of pump beams on polarization beats. Polarization beats, which originate from the interference between the macroscopic polarizations, have attracted a lot of attention recently [15–27]. It is closely related to the quantum beat spectroscopy, which appears in the conventional time-resolved fluorescence and in the time-resolved nonlinear laser spectroscopy. DeBeer *et al.* performed the first ultrafast modulation spectroscopy (UMS) experiment in sodium vapor [24]. Fu *et al.* [25,26] then analyzed the UMS with phase-conjugate geometry in a Doppler-broadened system by a second-order coherence-function theory. They found that a Doppler-free precision in the measurement of the energy-level splitting could be achieved.

In this paper, we have investigated the effects of Markovian field fluctuations in cascade three-level polarization beats. Based on three types of models described above, we have studied the influence of various quantities, such as laser linewidth, transverse relaxation rate, and longitudinal relaxation rate. One of the relevant problems is the stationary FWM with incoherent light sources, which is proposed by Morita and Yajima [28] to achieve an ultrafast temporal resolution of relaxation processes. Since they assume that laser linewidth is much longer than transverse relaxation rate, their theory cannot be used to study the effect of the light bandwidth on the Bragg reflection signal. Asaka *et al.* [29] have considered the finite linewidth effect. However, the constant background contribution has been ignored in their analysis. Our higher-order correlation on polarization beats (HOCPB) includes both the finite light bandwidth effect and constant background contribution. The different roles of the phase fluctuation and amplitude fluctuation have been pointed out in the time domain. If HOCPB is employed for the energy-level difference measurement, there are advantages that the energy-level difference can be widely separated and a Doppler-free precision in the measurement can be achieved. HOCPB is closely related to the Doppler-free saturated absorption spectroscopy (or two-photon absorption spectroscopy with a resonant intermediate state) and the three-pulse stimulated photon echo (or sum-frequency tri-level photon echo) when the pump beams are narrowband and broadband linewidth, respectively [21,22,25]. However, it possesses the main advantages of these techniques in the frequency domain and in the time domain.

II. BASIC THEORY

HOCPB is a polarization phenomenon [15,16] originating from the interference between one-photon and two-photon processes. Let us consider a cascade three-level system (Fig. 1) with a ground state $|0\rangle$, an intermediate state $|1\rangle$, and an excited state $|2\rangle$. States between $|0\rangle$ and $|1\rangle$ and between $|1\rangle$ and $|2\rangle$ are coupled by dipolar transition with resonant frequencies Ω_1 and Ω_2, respectively, while states between $|0\rangle$ and $|2\rangle$ are dipolar forbidden. We consider in this cascade three-level system a double-frequency time-delay FWM experiment in which beams *A* and *B* consist of two frequency components ω_1 and ω_2, while beam 3 has frequency ω_3 (Fig. 2). We assume that $\omega_1 \approx \Omega_1$ ($\omega_3 \approx \Omega_1$) and $\omega_2 \approx \Omega_2$, therefore ω_1 (ω_3) and ω_2 will drive the transitions from $|0\rangle$ to $|1\rangle$ and from $|1\rangle$ to $|2\rangle$, respectively. There are two processes involved in this double-frequency time-delay FWM. First the ω_1 frequency component of beams *A* and *B* induces population gratings of states $|0\rangle$ and $|1\rangle$, which are probed by beam 3 of frequency ω_3. This is a one-photon resonant degenerate FWM (DFWM) and the signal (beam 4) has frequency ω_3. Second, beam 3 and the ω_2 frequency component of beam *A* induce a two-photon coherence between $|0\rangle$ and $|2\rangle$, which is then probed by the ω_2 frequency component of beam *B*. This is a two-photon nondegenerate FWM (NDFWM) with a resonant intermediate state and the frequency of the signal equals ω_3 again.

The complex electric fields of beam *A*, E_{p1}, and beam *B*, E_{p2}, can be written as

$$E_{p1}=A_1(\vec{r},t)\exp(-i\omega_1 t)+A_2(\vec{r},t)\exp(-i\omega_2 t)$$
$$=\varepsilon_1 u_1(t)\exp[i(\vec{k}_1\cdot\vec{r}-\omega_1 t)]+\varepsilon_2 u_2(t)$$
$$\times\exp[i(\vec{k}_2\cdot\vec{r}-\omega_2 t)], \quad (1)$$

$$E_{P2}=A_1'(\vec{r},t)\exp(-i\omega_1 t)+A_2'(\vec{r},t)\exp(-i\omega_2 t)$$
$$=\varepsilon_1' u_1(t-\tau)\exp[i(\vec{k}_1'\cdot\vec{r}-\omega_1 t+\omega_1\tau)]$$
$$+\varepsilon_2' u_2(t-\tau)\exp[i(\vec{k}_2'\cdot\vec{r}-\omega_2 t+\omega_2\tau)], \quad (2)$$

here $\varepsilon_i,\vec{k}_i(\varepsilon_i',\vec{k}_i')$ are the constant field amplitude and the wave vector of the ω_i component in beam A (beam B), respectively. $u_i(t)$ is a dimensionless statistical factor that contains phase and amplitude fluctuations. τ is the time delay of beam B with respect to beam A. On the other hand, the complex electric fields of beam 3 can be written as

$$E_{P3}=A_3(\vec{r},t)\exp(-i\omega_3 t)=\varepsilon_3 u_3(t)\exp[i(\vec{k}_3\cdot\vec{r}-\omega_3 t)], \quad (3)$$

here ω_3, ε_3, and $\vec{k}_3$ are the frequency, the field amplitude, and the wave vector of beam 3, respectively. Since ω_1 and ω_3 come from the same laser source, we have $u_1(t)=u_3(t)$.

We employ perturbation theory to calculate the density-matrix elements. In the following perturbation chains

$$\text{(I)}\quad \rho_{00}^{(0)}\xrightarrow{A_1}\rho_{10}^{(1)}\xrightarrow{(A_1')^*}\rho_{00}^{(2)}\xrightarrow{A_3}\rho_{10}^{(3)},$$

$$\text{(II)}\quad \rho_{00}^{(0)}\xrightarrow{(A_1')^*}(\rho_{10}^{(1)})^*\xrightarrow{A_1}\rho_{00}^{(2)}\xrightarrow{A_3}\rho_{10}^{(3)},$$

$$\text{(III)}\quad \rho_{00}^{(0)}\xrightarrow{A_1}\rho_{10}^{(1)}\xrightarrow{(A_1')^*}\rho_{11}^{(2)}\xrightarrow{A_3}\rho_{10}^{(3)},$$

$$\text{(IV)}\quad \rho_{00}^{(0)}\xrightarrow{(A_1')^*}(\rho_{10}^{(1)})^*\xrightarrow{A_1}\rho_{11}^{(2)}\xrightarrow{A_3}\rho_{10}^{(3)},$$

$$\text{(V)}\quad \rho_{00}^{(0)}\xrightarrow{A_3}\rho_{10}^{(1)}\xrightarrow{A_2}\rho_{20}^{(2)}\xrightarrow{(A_2')^*}\rho_{10}^{(3)}.$$

Chains (I)–(IV) correspond to the one-photon resonant DFWM, while chain (V) corresponds to the two-photon resonant NDFWM.

Now, we consider the other possible perturbation chains, where the grating induced by beam 3 and ω_1 (or ω_2) frequency component of beam B is responsible for the generation of the FWM signal. These gratings have much smaller fringe spacings, which equal approximately one-half of the wavelengths of the incident lights. For a Doppler-broadened system, the gratings will be washed out by the atomic motion. Therefore, it is appropriate to neglect the FWM signal from these perturbation chains [26]. In addition, some perturbation chains involve the coherence between excited states $|1\rangle$ and $|2\rangle$. For a system with the relaxation time of ρ_{00} much longer than that of ρ_{21} (or ρ_{12}), the FWM signal can be reduced further. We have also neglected the contributions from the perturbation chains, which give rise to a signal with frequency $\omega_4=\pm(\omega_2-\omega_1)+\omega_3$, therefore, it can be separated from the FWM signal with frequency ω_3 by a monochromator or a narrow-band filter. Furthermore, the more strict requirement on the phase matching [27] and the involvement of ρ_{21} (or ρ_{12}) also make this process unimportant [26]. In addition, for the static grating (the FWM signal has the same frequency as the probe beam) the coherence length is usually longer than the thickness of a typical sample. For the moving grating [the signal from moving grating has the frequency $\omega_3\pm(\omega_2-\omega_1)$] the coherence length is usually much smaller than the thickness of a typical sample. In this case the contribution to the FWM signal from the moving grating can be neglected [27].

We obtain the third-order off-diagonal density-matrix element $\rho_{10}^{(3)}$ which has wave vector $\vec{k}_1-\vec{k}_1'+\vec{k}_3'$ or $\vec{k}_2-\vec{k}_2'+\vec{k}_3$. The nonlinear polarization $P^{(3)}$ responsible for the phase-conjugate FWM signal is given by averaging over the velocity distribution function $W(\vec{v})$. Thus $P^{(3)}=N\mu_1\int_{-\infty}^{+\infty}d\vec{v}\,w(\vec{v})\rho_{10}^{(3)}(\vec{v})$, here $\vec{v}$ is the atomic velocity, and N is the density of atoms. For a Doppler-broadened atomic system, we have $w(\vec{v})=(1/\sqrt{\pi}u)\exp[-(\vec{v}/u)^2]$.

The total polarization is $P^{(3)}=P^{(I)}+P^{(II)}+P^{(III)}+P^{(IV)}+P^{(V)}$. Here $P^{(I)}$, $P^{(II)}$, $P^{(III)}$, $P^{(IV)}$, and $P^{(V)}$ corresponding to polarization of the perturbation chain (I), (II), (III), (IV), and (V), respectively, are

$$P^{(\mathrm{I})}=S_1(\vec{r})\exp[-i(\omega_3 t+\omega_1\tau)]$$
$$\times\int_{-\infty}^{+\infty}d\vec{v}\,w(\vec{v})\int_0^\infty dt_3\int_0^\infty dt_2\int_0^\infty dt_1$$
$$\times\exp[-i\theta_{\mathrm{I}}(\vec{v})]H_1(t_1)H_2(t_2)H_3(t_3)$$
$$\times u_1(t-t_1-t_2-t_3)u_1^*(t-t_2-t_3-\tau)u_3(t-t_3), \quad (4)$$

$$P^{(\mathrm{II})}=S_1(\vec{r})\exp[-i(\omega_3 t+\omega_1\tau)]$$
$$\times\int_{-\infty}^{+\infty}d\vec{v}\,w(\vec{v})\int_0^\infty dt_3\int_0^\infty dt_2\int_0^\infty dt_1$$
$$\times\exp[-i\theta_{\mathrm{II}}(\vec{v})]H_1^*(t_1)H_2(t_2)H_3(t_3)$$
$$\times u_1(t-t_2-t_3)u_1^*(t-t_1-t_2-t_3-\tau)u_3(t-t_3), \quad (5)$$

$$P^{(\mathrm{III})}=S_1(\vec{r})\exp[-i\omega_3 t-i\omega_1\tau]$$
$$\times\int_{-\infty}^{+\infty}d\vec{v}\,w(\vec{v})\int_0^\infty dt_3\int_0^\infty dt_2\int_0^\infty dt_1$$
$$\times\exp[-i\theta_{\mathrm{I}}(\vec{v})]H_1(t_1)H_4(t_2)H_3(t_3)$$
$$\times u_1(t-t_1-t_2-t_3)u_1^*(t-t_2-t_3-\tau)u_3(t-t_3), \quad (6)$$

$$P^{(\mathrm{IV})}=S_1(\vec{r})\exp[-i\omega_3 t-i\omega_1\tau]\times\int_{-\infty}^{\infty}d\vec{\nu}\,w(\vec{\nu})\int_0^{\infty}dt_3\int_0^{\infty}dt_2\int_0^{\infty}dt_1\times\exp[-i\theta_{\mathrm{II}}(\vec{\nu})]H_1^*(t_1)H_4(t_2)H_3(t_3)\times u_1(t-t_2-t_3)u_1^*(t-t_1-t_2-\tau_3-\tau)u_3(t-t_3),\quad(7)$$

$$P^{(\mathrm{V})}=S_2(\vec{r})\exp[-i\omega_3 t-i\omega_2\tau]\times\int_{-\infty}^{+\infty}d\vec{\nu}\,w(\vec{\nu})\int_0^{\infty}dt_3\int_0^{\infty}dt_2\int_0^{\infty}dt_1\times\exp[-i\theta_{\mathrm{III}}(\vec{\nu})]H_3(t_1)H_5(t_2)H_3(t_3)\times u_2(t-t_2-t_3)u_2^*(t-t_3-\tau)u_3(t-t_1-t_2-t_3),\quad(8)$$

here

$$S_1(\vec{r})=-i\hbar N\left(\frac{\mu_1}{\hbar}\right)^4\varepsilon_1(\varepsilon_1')^*\varepsilon_3\exp[i(\vec{k}_1-\vec{k}_1'+k_3)\cdot\vec{r}],$$

$$S_2(\vec{r})=-i\hbar N\left(\frac{\mu_1}{\hbar}\right)^2\left(\frac{\mu_2}{\hbar}\right)^2\varepsilon_2(\varepsilon_2')^*\varepsilon_3\times\exp[i(\vec{k}_2-\vec{k}_2'+\vec{k}_3)\cdot\vec{r}],$$

$$\theta_{\mathrm{I}}(\vec{\nu})=\vec{\nu}\cdot[\vec{k}_1(t_1+t_2+t_3)-\vec{k}_1'(t_2+t_3)+\vec{k}_3t_3],$$

$$\theta_{\mathrm{II}}(\vec{\nu})=\vec{\nu}\cdot[-\vec{k}_1'(t_1+t_2+t_3)+\vec{k}_1(t_2+t_3)+\vec{k}_3t_3],$$

$$\theta_{\mathrm{III}}(\vec{\nu})=\vec{\nu}\cdot[\vec{k}_3(t_1+t_2+t_3)+\vec{k}_2(t_1+t_2)-\vec{k}_2't_3],$$

$$H_1(t)=\exp[-(\Gamma_{10}+i\Delta_1)t],\quad H_2(t)=\exp(-\Gamma_0 t),$$

$$H_3(t)=\exp[-(\Gamma_{10}+i\Delta_3)t],\quad H_4(t)=\exp(-\Gamma_1 t),$$

$$H_5(t)=\exp[-(\Gamma_{20}+i\Delta_2+i\Delta_3)t],\quad \mu_1\ (\mu_2)$$

is the dipole-moment matrix element between $|0\rangle$ and $|1\rangle$ ($|1\rangle$ and $|2\rangle$), Γ_0 (Γ_1) is the population relaxation rate of state $|0\rangle$ ($|1\rangle$), Γ_{10} (Γ_{20}) is the transverse relaxation rate of the transition from $|0\rangle$ to $|1\rangle$ ($|0\rangle$ to $|2\rangle$), and $\Delta_1=\Omega_1-\omega_1$, $\Delta_2=\Omega_2-\omega_2$, and $\Delta_3=\Omega_1-\omega_3$.

The FWM signal is proportional to the average of the absolute square of $P^{(3)}$ over the random variable of the stochastic process $\langle|P^{(3)}|^2\rangle$, which involves sixth-, fourth-, and second-order coherence function of $u_i(t)$ in phase-conjugation geometry, while the FWM signal intensity in self-diffraction geometry is related to the sixth-order coherence function of the incident fields [24]. For the macroscopic system where phase matching takes place, this signal must be drawn from the $P^{(3)}$ developed on one ''atom'' multiplied by the $(P^{(3)})^*$ that is developed on another ''atom,'' which must be located elsewhere in space (with summation over all such pairs) [8,12]. We first assume that the laser sources are multimode thermal sources. $u_i(t)$ has Gaussian statistics with its sixth-and fourth-order coherence function satisfying [6,7]

$$\langle u_i(t_1)u_i(t_2)u_i(t_3)u_i^*(t_4)u_i^*(t_5)u_i^*(t_6)\rangle=\langle u_i(t_1)u_i^*(t_4)\rangle\langle u_i(t_2)u_i(t_3)u_i^*(t_5)u_i^*(t_6)\rangle+\langle u_i(t_1)u_i^*(t_5)\rangle\langle u_i(t_2)u_i(t_3)u_i^*(t_4)u_i^*(t_6)\rangle+\langle u_i(t_1)u_i^*(t_6)\rangle\langle u_i(t_2)u_i(t_3)u_i^*(t_4)u_i^*(t_5)\rangle,\quad(9)$$

and

$$\langle u_i(t_1)u_i(t_2)u_i^*(t_3)u_i^*(t_4)\rangle=\langle u_i(t_1)u_i^*(t_3)\rangle\langle u_i(t_2)u_i^*(t_4)\rangle+\langle u_i(t_1)u_i^*(t_4)\rangle\times\langle u_i(t_2)u_i^*(t_3)\rangle.\quad(10)$$

Furthermore assuming that the laser sources in beams *A*, *B*, and 3 have Lorentzian line shape, then we have

$$\langle u_i(t_1)u_i^*(t_2)\rangle=\exp(-\alpha_i|t_1-t_2|),\quad(11)$$

here $\alpha_i=1/2\delta\omega_i$ with $\delta\omega_i$ the linewidth of the laser with frequency ω_i. The form of the second-order coherence function, which is determined by the laser line shape, as expressed in Eq. (11), is general feature of the three different stochastic models [6,7].

We now consider the case that the laser sources are narrowband so that $\alpha_1,\alpha_2\ll\Gamma_{10},\Gamma_{20}$ and $\Gamma_0,\Gamma_1\ll\Gamma_{10},\Gamma_{20}$. For simplicity, here we neglect the Doppler effect. Performing the tedious integration, the beat signal intensity then becomes

$$I(\tau,r)\propto\langle|P^{(3)}|^2\rangle\propto B_1+|\eta|^2B_2+B_3\exp(-2\alpha_1|\tau|)+|\eta|^2B_2\exp(-2\alpha_2|\tau|)+\exp[-(\alpha_1+\alpha_2)|\tau|]\times B_2B_3\{\eta\exp[i\Delta\vec{k}\cdot\vec{r}+i(\omega_2-\omega_1)\tau]+\eta^*\times\exp[-i\Delta\vec{k}\cdot\vec{r}-i(\omega_2-\omega_1)\tau]\},\quad(12)$$

where $\Delta\vec{k}=(\vec{k}_1-\vec{k}_1')-(\vec{k}_2-\vec{k}_2')$, $\eta=\mu_2^2/\mu_1^2[\varepsilon_2^*\varepsilon_2'/\varepsilon_1^*\varepsilon_1']$, B_1, B_2, and B_3 mainly depending on the laser linewidths and relaxation rate of the transition are constants.

Relation (12) consist of five terms. The first and third terms are dependent on the $u_1(t)$ sixth-order coherence function for DFWM, while the second and fourth terms are dependent on the $u_2(t)$ fourth- and $u_1(t)$ second-order coherence functions for NDFWM. The first and second terms originating from the amplitude fluctuation of the chaotic field are independent of the relative time delay between the two beams *A* and *B*. The third and fourth terms indicate an exponential decay of the beat signal as $|\tau|$ increases. The fifth term depending on the $u_1(t)$ fourth- and $u_2(t)$ second-order coherence functions, gives rise to the modulation of the beat signal.

Equation (12) indicates that beat signal oscillates not only temporally but also spatially with a period $2\pi/\Delta k$ along the

direction $\Delta\vec{k}$, which is almost perpendicular to the propagation direction of the beat signal, here $\Delta k \approx 2\pi|\lambda_1 - \lambda_2|\theta/\lambda_2\lambda_1$, θ is the angle between beam *A* and beam *B*. Physically, the polarization-beat model assumes that both the pump beams are plane waves. Therefore DFWM and NDFWM, which propagate along $\vec{k}_{s_1}=\vec{k}_1-\vec{k}_1'+\vec{k}_3$ and $\vec{k}_{s_2}=\vec{k}_2-\vec{k}_2'+\vec{k}_3$, respectively, are plane waves also. Since DFWM and NDFWM propagate along a slightly different direction, the interference between them leads to the spatial oscillation. Equation (12) also indicates that beat signal modulates temporally with a frequency $\omega_2-\omega_1$ as τ is varied. In this case when ω_1 and ω_2 are tuned to the resonant frequencies of the transitions from $|0\rangle$ to $|1\rangle$ and from $|1\rangle$ and $|2\rangle$, respectively, the modulation frequency equals $\Omega_2-\Omega_1$. In the other words, we can obtain beating between the resonant frequencies of a cascade three-level system. A Doppler-free precision can be achieved in the measurement of $\Omega_2-\Omega_1$ [17,19].

III. HOCPB IN A DOPPLER-BROADENED SYSTEM

The beat signal can be calculated from a different viewpoint. Under the Doppler-broadened limit (i.e., $k_3u\rightarrow\infty$), we have

$$\int_{-\infty}^{+\infty} d\vec{\nu}\, w(\vec{\nu})\exp[-i\theta_{\mathrm{I}}(\vec{\nu})]\approx\frac{2\sqrt{\pi}}{k_3u}\,\delta(t_3-\xi_1t_1), \quad (13)$$

$$\int_{-\infty}^{+\infty} d\vec{\nu}\, w(\vec{\nu})\exp[-i\theta_{\mathrm{II}}(\vec{\nu})]\approx\frac{2\sqrt{\pi}}{k_3u}\,\delta(t_3+\xi_1t_1), \quad (14)$$

$$\int_{-\infty}^{+\infty} d\vec{\nu}\, w(\vec{\nu})\exp[-i\theta_{\mathrm{III}}(\vec{\nu})]\approx\frac{2\sqrt{\pi}}{k_3u}\,\delta(t_1+t_2+t_3-\xi_2t_2), \quad (15)$$

here we assume $\xi_2>1$, $\xi_1=k_1/k_3$, $\xi_2=k_2/k_3$. When we substitute Eqs. (13)–(15) into Eqs. (4)–(8) we obtain

$$I(\tau,r)\propto\langle|P^{(3)}|^2\rangle=\langle|P^{(\mathrm{I})}+P^{(\mathrm{II})}+P^{(\mathrm{V})}|^2\rangle. \quad (16)$$

We first consider the case that the laser sources are narrowband so that $\alpha_1,\alpha_2\ll\Gamma_{10},\Gamma_{20}$ and $\Gamma_0,\Gamma_1\ll\Gamma_{10},\Gamma_{20}$. Performing the tedious integration, the beat signal intensity is

$$\begin{aligned} I(\tau,r)\propto\langle|P^{(3)}|^2\rangle&=B_4+B_5|\eta|^2+B_6\exp(-2\alpha_1|\tau|)\\ &+|\eta|^2B_7\exp(-2\alpha_2|\tau|)+\exp[-(\alpha_1+\alpha_2)|\tau|]\\ &\times B_6B_7\{\eta\exp[i\Delta\vec{k}\cdot\vec{r}+i(\omega_2-\omega_1)\tau]+\eta^*\\ &\times\exp[-i\Delta\vec{k}\cdot\vec{r}-i(\omega_2-\omega_1)\tau]\}, \end{aligned} \quad (17)$$

where B_4, B_5, B_6, and B_7 mainly depending on the laser linewidths and relaxation rate of the transition are constants. This equation is consistent with Eq. (12).

We now consider the case that the laser sources are broadband so that $\alpha_1,\alpha_2\gg\Gamma_{10},\Gamma_{20}\gg\Gamma_0,\Gamma_1$. In this case, the beat signal rises to its maximum quickly and then decays with time constant mainly determined by the transverse relaxation times of the system. Although the beat signal modulation is complicated in general, at the tail of the signal (i.e., $|\tau|\gg\alpha_1^{-1}$, $|\tau|\gg\alpha_2^{-1}$) we have

(i) $\tau>0$

$$\begin{aligned} I(\tau,r)\propto\langle|P^{(3)}|^2\rangle&=B_8+|\eta|^2B_9+B_{10}\exp(-2\Gamma_{10}^a|\tau|)\\ &+|\eta|^2B_{11}\exp[-2(\Gamma_{20}^a-\Gamma_{10})|\tau|]+B_{10}B_{11}\\ &\times\exp[-(\Gamma_{20}^a+\Gamma_{10}^a-\Gamma_{10})|\tau|]\\ &\times\{\eta\exp[i\Delta\vec{k}\cdot\vec{r}+i(\Omega_2-\Omega_1)\tau\\ &-i(\xi_2-\xi_1)\Delta_3\tau]+\eta^*\\ &\times\exp[-i\Delta\vec{k}\cdot\vec{r}-i(\Omega_2-\Omega_1)\tau+i(\xi_2-\xi_1)\Delta_3\tau]\}, \end{aligned} \quad (18)$$

where B_8, B_9, B_{10}, and B_{11} mainly depending on the laser linewidths and relaxation rate of the transition, are constants, $\Gamma_{10}^a=\Gamma_{10}+\xi_1\Gamma_{10}$, $\Gamma_{20}^a=\Gamma_{20}+\xi_2\Gamma_{10}$.

Relation (18) also consist of five terms. The first and third terms are dependent on the $u_1(t)$ sixth-order coherence function for DFWM, while the second and fourth terms are dependent on the $u_2(t)$ fourth- and $u_1(t)$ second-order coherence functions for NDFWM. The first and second terms originating from the amplitude fluctuation of the chaotic field are independent of the relative time delay between the two beams *A* and *B*. The third and fourth terms indicate an exponential decay of the beat signal as $|\tau|$ increases. The fifth term, depending on the $u_1(t)$ fourth- and $u_2(t)$ second-order coherence functions, gives rise to the modulation of the beat signal. Equation (18) indicates that the modulation frequency of the beat signal equals $\Omega_2-\Omega_1$, when $\Delta_3=0$. The overall accuracy of using HOCPB with broadband lights to measure the energy-level difference of the excited states is limited by the homogeneous linewidths [17,19].

(ii) $\tau<0$

$$\begin{aligned} I(\tau,r)\propto\langle|P^{(3)}|^2\rangle&=B_8+B_9|\eta|^2+B_{12}\exp(-2\alpha_1|\tau|)\\ &+|\eta|^2B_{13}\exp(-2\alpha_2|\tau|)+\exp[-(\alpha_1+\alpha_2)|\tau|]\\ &\times B_{12}B_{13}\{\eta\exp[i\Delta\vec{k}\cdot\vec{r}+i(\omega_2-\omega_1)\tau]+\eta\\ &\times\exp[-i\Delta\vec{k}\cdot\vec{r}-i(\omega_2-\omega_1)\tau]\}, \end{aligned} \quad (19)$$

where, B_{12} and B_{13}, mainly depending on the laser linewidths and relaxation rate of the transition, are constants. This equation is consistent with Eq. (12). The requirement for the existence of a τ-dependent beat signal for $\tau<0$ is that the phase-correlated subpulses in beams *A* and *B* are overlapped temporally. Since beams *A* and *B* are mutually coherent, the temporal behavior of the beat signal should coincide with the case when the beams *A* and *B* are nearly monochromatic [17,19].

IV. PHOTON ECHO

It is interesting to understand the underlying physics in HOCPB with broadband nontransform limited quasi-cw (noisy) lights [28,29]. Much attention has been paid to the

study of various ultrafast phenomena by using incoherent light sources recently [8–14,30]. For the phase-matching condition $\vec{k}_1-\vec{k}_1'+\vec{k}_3$, the three-pulse stimulated photon-echo exists for the perturbation chain (I) and (III). For the phase-matching condition $\vec{k}_2-\vec{k}_2'+\vec{k}_3$ the sum-frequency tri-level echo exists for the perturbation chain (V) [21,22,25].

A. The chaotic field

The chaotic field is a complex Gaussian stochastic process. Under the Doppler-broadened limit (i.e., $k_3u\rightarrow\infty$), if assuming that the laser source has Gaussian line shape, then we have

$$\langle u_i(t_1)u_i^*(t_2)\rangle=\exp\left\{-\left[\frac{\alpha_i}{2\sqrt{\ln 2}}(t_1-t_2)\right]^2\right\}$$
$$=\exp\{-[\beta_i(t_1-t_2)]^2\}.$$

We now consider the case that the laser sources are broadband so that $\alpha_1,\alpha_2\gg\Gamma_{10}$, $\Gamma_{20}\gg\Gamma_0,\Gamma_1$, then

$$\langle u_i(t_1)u_i^*(t_2)\rangle=\exp[-\beta_i^2(t_1-t_2)^2]\approx\frac{\sqrt{\pi}}{\beta_i}\delta(t_1-t_2). \tag{20}$$

When we substitute Eqs. (9), (10), and (20) into Eqs. (16) we obtain as follows
(i) $\tau>0$

$$\begin{aligned}I(\tau,r)\propto\langle|P^{(3)}|^2\rangle=&A_1+|\eta|^2A_2+|A_3|^2\exp(-2\Gamma_{10}^a|\tau|)\\&+|A_4|^2\exp[-2(\Gamma_{20}^a-\Gamma_{10})|\tau|]\\&+A_3A_4\exp[-\alpha_1|\xi_1-\xi_2\|\tau|]\\&\times\exp[-(\Gamma_{20}^a+\Gamma_{10}^a-\Gamma_{10})|\tau|]\\&\times\{\eta\exp[i\Delta\vec{k}\cdot\vec{r}+i(\Omega_2-\Omega_1)\tau\\&+i(\xi_2-\xi_1)\Delta_3\tau]+\eta^*\\&\times\exp[-i\Delta\vec{k}\cdot\vec{r}-i(\Omega_2-\Omega_1)\tau\\&-i(\xi_2-\xi_1)\Delta_3\tau]\},\end{aligned} \tag{21}$$

where

$$A_1=\frac{2}{\alpha_1^2\Gamma_{10}^a\xi_1}\left(\frac{\Gamma_0+\Gamma_1}{2\Gamma_0\Gamma_1}+\frac{1}{\Gamma_0+\Gamma_1}\right),$$

$$A_2=\frac{\xi_2-1}{\alpha_2^2(\Gamma_{20}^a-\Gamma_{10})^2},\quad A_3=\frac{2}{\alpha_1}\frac{\Gamma_0+\Gamma_1}{\Gamma_0\Gamma_1},$$

$A_4=2/\alpha_2(\xi_2-1)|\tau|$. This equation is analogous to Eq. (18).
(ii) $\tau<0$

$$I(\tau,r)\propto\langle|P^{(3)}|^2\rangle=A_1+|\eta|^2A_2+\frac{4}{\Gamma_{10}(\xi_1+1)^2\alpha_1^3}$$
$$\times\{\exp(-2\Gamma_0|\tau|)+\exp(-2\Gamma_1|\tau|)$$
$$+2\exp[-(\Gamma_0+\Gamma_1)|\tau|]\}.$$

Photon echo does not exist for the perturbation chain (I), (III), and (V). The requirement for the existence of a τ-dependent beat signal for $\tau<0$ is that the phase-correlated subpulses in beams A and B are overlapped temporally. Since beams A and B are mutually coherent, the temporal behavior of the beat signal should coincide with the case when the beams A and B are nearly monochromatic [17,19]. Therefore, this case is consistent with Eq. (12).

B. The phase-diffusion field

We have assumed that the laser sources are chaotic field in the above calculation. A chaotic field, which is used to describe a multimode laser source, is characterized by the fluctuation of both the amplitude and the phase of the field. Another commonly used stochastic model is the phase-diffusion model, which is used to describe a amplitude-stabilized laser source. This model assumes that the amplitude of the laser field is a constant, while its phase fluctuates as a random process caused by spontaneous emission. If the lasers have Lorentzian line shape, the sixth- and fourth-order coherence function are [6,7]

$$\begin{aligned}&\langle u_i(t_1)u_i(t_2)u_i(t_3)u_i^*(t_4)u_i^*(t_5)u_i^*(t_6)\rangle\\&=\exp[-\alpha_i(|t_1-t_4|+|t_1-t_5|+|t_1-t_6|+|t_2-t_4|\\&\quad+|t_2-t_5|+|t_2-t_6|+|t_3-t_4|\\&\quad+|t_3-t_5|+|t_3-t_6|)]\exp[\alpha_i(|t_1-t_2|+|t_1-t_3|\\&\quad+|t_2-t_3|+|t_4-t_5|+|t_4-t_6|+|t_5-t_6|)],\end{aligned} \tag{22}$$

and

$$\begin{aligned}&\langle u_i(t_1)u_i(t_2)u_i^*(t_3)u_i^*(t_4)\rangle\\&=\exp[-\alpha_i(|t_1-t_3|+|t_1-t_4|+|t_2-t_3|+|t_2-t_4|)]\\&\quad\times\exp[\alpha_i(|t_1-t_2|+|t_3-t_4|)].\end{aligned} \tag{23}$$

We now consider the case that the laser sources are broadband so that $\alpha_1,\alpha_2\gg\Gamma_{10}$, $\Gamma_{20}\gg\Gamma_0,\Gamma_1$. Then

$$\langle u_i(t_1)u_i^*(t_2)\rangle=\exp(-\alpha_i|t_1-t_2|)\approx\frac{2}{\alpha_i}\delta(t_1-t_2)\quad(i=1,2). \tag{24}$$

When we substitute Eqs. (22)–(24) into Eq. (16) we obtain as follows
(i) $\tau>0$

$$I(\tau,r)\propto\langle|P^{(3)}|^2\rangle=|A_5|^2\exp(-2\Gamma_{10}^a|\tau|)+|\eta A_6|^2\times\exp[-2(\Gamma_{20}^a-\Gamma_{10})|\tau|]+A_5A_6\times\exp[-\alpha_1|\xi_1-\xi_2\|\tau|]\times\exp[-(\Gamma_{20}^a+\Gamma_{10}^a-\Gamma_{10})|\tau|]\times\{\eta\exp[i\Delta\vec{k}\cdot\vec{r}+i(\Omega_2-\Omega_1)\tau+i(\xi_2-\xi_1)\Delta_3\tau]+\eta^*\exp[-i\Delta\vec{k}\cdot\vec{r}-i(\Omega_2-\Omega_1)\times\tau-i(\xi_2-\xi_1)\Delta_3\tau]\},\quad(25)$$

where $A_5=(\Gamma_0+\Gamma_1)/\alpha_1\Gamma_0\Gamma_1$, $A_6=\tau(\xi_2-1)/\alpha_2$.
(ii) $\tau<0$

$$I(\tau,r)\propto\langle|P^{(3)}|^2\rangle=\frac{4}{\Gamma_{10}^a\alpha_1^3\xi_1}\{\exp(-2\Gamma_0|\tau|)+\exp(-2\Gamma_1|\tau|)+2\times\exp[-(\Gamma_0+\Gamma_1)|\tau|]\}.$$

Photon echo doesn't exist for the perturbation chains (I), (III), and (V).

Relation (25) consist of three terms. The first term is dependent on the $u_1(t)$ sixth-order coherence function for DFWM, while the second term is dependent on the $u_2(t)$ fourth- and $u_1(t)$ second-order coherence functions for NDFWM. The first and second terms indicate an exponential decay of the beat signal as $|\tau|$ increases. The third term depending on the $u_1(t)$ fourth- and $u_2(t)$ second-order coherence functions gives rise to the modulation of the beat signal. This case is consistent with the results of the second-order coherence function theory [17,25,26]; the constant background contribution has been ignored in their analysis. Therefore, the sixth-order coherence function theory of chaotic field is of vital importance in HOCPB.

C. The Gaussian-amplitude field

The Gaussian-amplitude field has a constant phase but its real amplitude undergoes Gaussian fluctuations. If the lasers have Lorentzian line shape, the sixth- and fourth-order coherence function are [6,7]

$$\langle u_i(t_1)u_i(t_2)u_i(t_3)u_i(t_4)u_i(t_5)u_i(t_6)\rangle=\langle u_i(t_1)u_i(t_4)\rangle\times\langle u_i(t_2)u_i(t_3)u_i(t_5)u_i(t_6)\rangle+\langle u_i(t_1)u_i(t_5)\rangle\times\langle u_i(t_2)u_i(t_3)u_i(t_4)u_i(t_6)\rangle+\langle u_i(t_1)u_i(t_6)\rangle\times\langle u_i(t_2)u_i(t_3)u_i(t_4)u_i(t_5)\rangle+\langle u_i(t_1)u_i(t_2)\rangle\times\langle u_i(t_3)u_i(t_4)u_i(t_5)u_i(t_6)\rangle+\langle u_i(t_1)u_i(t_3)\rangle\times\langle u_i(t_2)u_i(t_4)u_i(t_5)u_i(t_6)\rangle,\quad(26)$$

and

$$\langle u_i(t_1)u_i(t_2)u_i(t_3)u_i(t_4)\rangle=\langle u_i(t_1)u_i(t_3)\rangle\langle u_i(t_2)u_i(t_4)\rangle+\langle u_i(t_1)u_i(t_4)\rangle\times\langle u_i(t_2)u_i(t_3)\rangle+\langle u_i(t_1)u_i(t_2)\rangle\times\langle u_i(t_3)u_i(t_4)\rangle.\quad(27)$$

When we substitute Eqs. (24), (26), and (27) into Eqs. (16) we obtain as follows
(i) $\tau>0$

$$I(\tau,r)\propto\langle|P^{(3)}|^2\rangle=A_7+|\eta|^2A_8+\exp(-2\Gamma_{10}^a|\tau|)\{A_9+A_{10}(\exp[-(2\xi_1-1)\Gamma_0|\tau|]-\exp[-(2\xi_1+1)\Gamma_0|\tau|])+A_{11}(\exp[-(2\xi_1-1)\Gamma_1|\tau|]-\exp[-(2\xi_1+1)\Gamma_1|\tau|])\}+A_{12}\exp[-2(\Gamma_{20}^a-\Gamma_{10})|\tau|]+A_{13}\exp[-\alpha_1|\xi_1-\xi_2\|\tau|]\times\exp[-(\Gamma_{20}^a+\Gamma_{10}^a-\Gamma_{10})|\tau|]\{\eta\exp[i\Delta\vec{k}\cdot\vec{r}+i(\Omega_2-\Omega_1)\tau+i(\xi_2-\xi_1)\Delta_3\tau]+\eta^*\exp[-i\Delta\vec{k}\cdot\vec{r}-i(\Omega_2-\Omega_1)\tau-i(\xi_2-\xi_1)\Delta_3\tau]\},\quad(28)$$

where

$$A_7=\frac{4}{\alpha_1^2}\frac{\Gamma_0^2+\Gamma_1^2+6\Gamma_0\Gamma_1}{\Gamma_{10}^a\Gamma_0\Gamma_1(\Gamma_0+\Gamma_1)},\quad A_8=\frac{4(\xi_2-1)}{(\alpha_2\Gamma_{20}^a)^2},$$

$$A_9=\frac{4(\xi_1+1)}{\alpha_1^2(2\xi_1+1)}\frac{(\Gamma_0+\Gamma_1)^2}{\Gamma_0^2\Gamma_1^2},$$

$$A_{10}=\frac{3\Gamma_0+\Gamma_1}{2\Gamma_0^2(\Gamma_0+\Gamma_1)},\quad A_{11}=\frac{3\Gamma_1+\Gamma_0}{2\Gamma_1^2(\Gamma_0+\Gamma_1)},$$

$$A_{12}=(\xi_2-1)^2|\tau|^2+\frac{\xi_2+1}{4(\Delta_2+\xi_2\Delta_3)^2},$$

$$A_{13}=\frac{4(\xi_2-1)|\tau|}{\alpha_1\alpha_2}\frac{\Gamma_0+\Gamma_1}{\Gamma_0\Gamma_1}.$$

(ii) $\tau<0$, $I(\tau,r)\propto\langle|P^{(3)}|^2\rangle=A_7+|\eta|^2A_8$. Photon echo doesn't exist for the perturbation chains (I), (III), and (V).

Relation (28) consist of five terms. The first and third terms are dependent on the $u_1(t)$ sixth-order coherence function for DFWM, while the second and fourth terms are dependent on the $u_2(t)$ fourth- and $u_1(t)$ second-order coherence functions for NDFWM. The first and second terms originating from the amplitude fluctuation of the Gaussian-amplitude field are independent of the relative time delay between the two beams *A* and *B*. The third and fourth terms

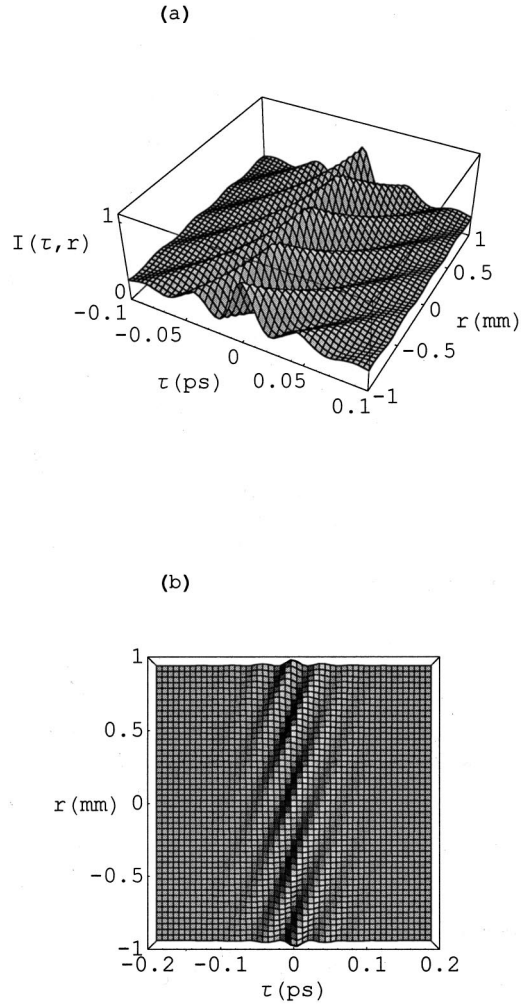

FIG. 3. (a) A three-dimensional plot of the beat signal intensity $I(\tau,r)$ versus time delay τ and transverse distance r for the Gaussian-amplitude field. The parameters are $\Omega_2-\Omega_1=140\ \mathrm{ps}^{-1}$, $\Delta k=12.25\ \mathrm{mm}^{-1}$, $\eta=\xi_i=1$, $A_i=0.6$, $\Gamma^a_{10}=13.5\ \mathrm{ps}^{-1}$, $\Gamma^a_{20}-\Gamma_{10}=14.5\ \mathrm{ps}^{-1}$, $\Gamma_0=2.7\ \mathrm{ps}^{-1}$, and $\Gamma_1=2.9\ \mathrm{ps}^{-1}$. (b) A two-dimensional representation of the beat signal intensity $I(\tau,r)$.

indicate an exponential decay of the beat signal as $|\tau|$ increases. The fifth term depending on the $u_1(t)$ fourth- and $u_2(t)$ second-order coherence functions gives rise to the modulation of the beat signal. Equation (28) also indicates that beat signal oscillates not only temporally with a period $2\pi/|\Omega_2-\Omega_1|=44.9\,\mathrm{fs}$ but also spatially with a period $2\pi/\Delta k=0.51\,\mathrm{mm}$ along the direction $\Delta\vec{k}$, which is almost perpendicular to the propagation direction of the beat signal (Fig. 3). The three-dimensional plot of the beat signal intensity $I(\tau,r)$ versus time delay τ and transverse distance r has larger constant background caused by the intensity fluctuation of the Gaussian-amplitude field. At zero relative time delay ($\tau=0$), the twin beams originating from the same source enjoy perfect overlap at the sample of their corresponding noise patterns. This gives maximum interferometric contrast. As $|\tau|$ is increased, the interferometric contrast diminishes on the time scale that reflects material memory, usually much longer than the correlation time of the light [13].

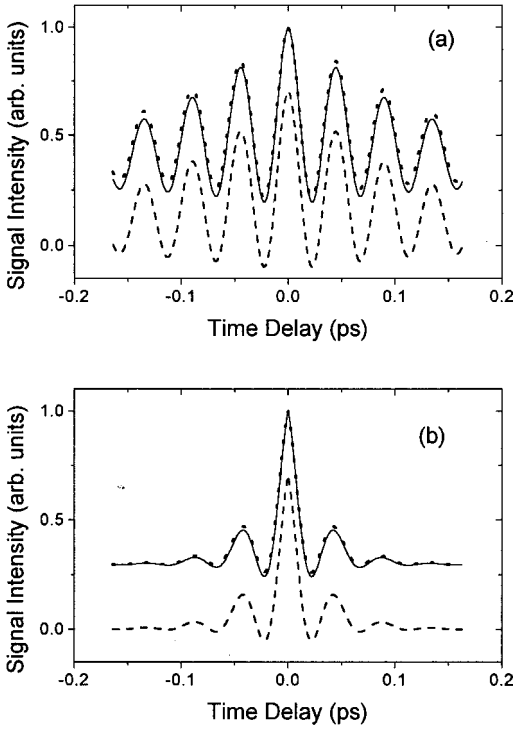

FIG. 4. The beat signal intensity versus relative time delay. The three curves represent the chaotic field (solid line), phase-diffusion field (dashed line), and Gaussian-amplitude field (dotted line). The parameters are $\Omega_2-\Omega_1=140\ \mathrm{ps}^{-1}$, $\Delta k=0$, $\eta=\xi_i=1$, $A_i=0.6$, while $\Gamma^a_{10}=2.7\ \mathrm{ps}^{-1}$, $\Gamma^a_{20}-\Gamma_{10}=2.9\ \mathrm{ps}^{-1}$, $\Gamma_0=1.35\ \mathrm{ps}^{-1}$, $\Gamma_1=1.45\ \mathrm{ps}^{-1}$ for (a) and $\Gamma^a_{10}=13.5\ \mathrm{ps}^{-1}$, $\Gamma^a_{20}-\Gamma_{10}=14.5\ \mathrm{ps}^{-1}$, $\Gamma_0=2.7\ \mathrm{ps}^{-1}$, and $\Gamma_1=2.9\ \mathrm{ps}^{-1}$ for (b).

It is important to note that these three types of fields can have the same spectral density and thus the same second-order coherence function. The fundamental differences in the statistics of these fields are manifest only in the higher-order coherence functions. The term ''higher-order'' refers to all orders larger than the second. According to Gaussian statistics, a chaotic field can be completely described by second-order coherence function. But the phase-diffusion field and Gaussian-amplitude field require all order coherence functions [6,7]. In this paper, different stochastic models of the laser field only affect the sixth- and fourth-order coherence

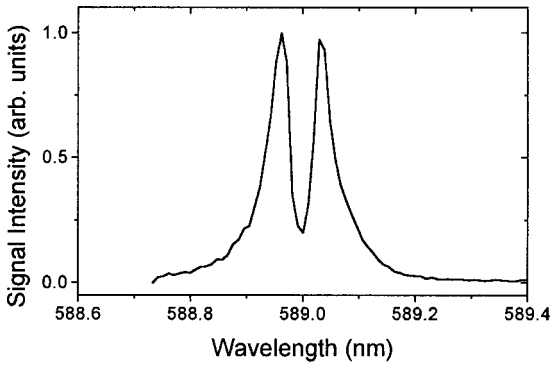

FIG. 5. Spectrum of DFWM when beams A and B consist of only ω_1 in which center wavelength is 589 nm.

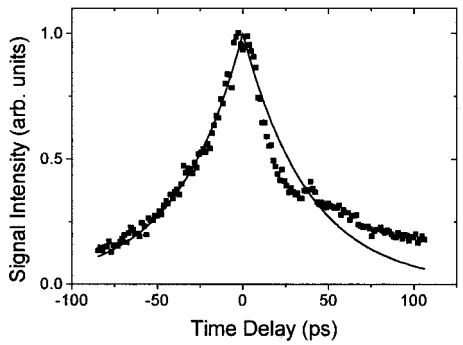

FIG. 6. DFWM signal intensity versus relative time delay when beams *A* and *B* consist of only ω_1. The square is the experimental data; the solid curve is the theoretical curve with $\alpha_1 = 2.7\times10^{10}\ \mathrm{s}^{-1}$, $B_1 = 0.1$, and $B_3 = 1$.

functions [20]. Figure 4 presents the beat signal intensity versus relative time delay. The three curves represent the chaotic field (solid line), phase-diffusion field (dashed line), and Gaussian-amplitude field (dotted line). The polarization beat signal is shown to be particularly sensitive to the statistical properties of the Markovian stochastic light fields with arbitrary bandwidth. This is quite different from the fourth-order partial-coherence effects in the formation of integrated-intensity gratings with pulsed light sources [31]. Their results proved to be insensitive to the specific radiation models. The constant background of the beat signal for a Gaussian-amplitude field or a chaotic field is much larger than that of the signal for a phase-diffusion field in Fig. 4. The physical explanation for this is that the Gaussian-amplitude field undergoes stronger intensity fluctuations than a chaotic field. On the other hand, the intensity (amplitude) fluctuations of the Gaussian-amplitude field or the chaotic field are always much larger than the pure phase fluctuations of the phase-diffusion field.

The main purpose of the above discussion is that we reveal an important fact that the amplitude fluctuation plays a critical role in the temporal behavior of the HOCPB signal. Furthermore, the different roles of the phase fluctuation and amplitude fluctuation have been pointed out in the time domain. This is quite different from the time delayed FWM with incoherent light in a two-level system [28]. For the latter case, the phase fluctuation of the light field is crucial. But the HOCPB is analogous to the Raman-enhanced polar-

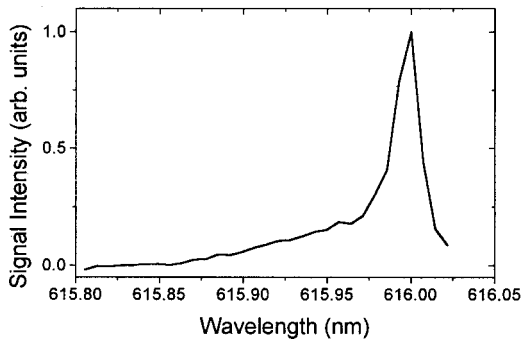

FIG. 7. Spectrum of NDFWM when beams *A* and *B* consist of only ω_2 in which center wavelength is 616 nm.

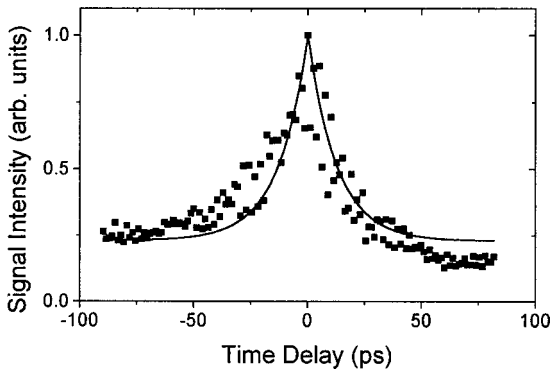

FIG. 8. NDFWM signal intensity versus relative time delay when beams *A* and *B* consist of only ω_2. The square is the experimental data; the solid curve is the theoretical curve with $\alpha_2 = 2.9\times10^{10}\ \mathrm{s}^{-1}$, $B_2 = 0.2$, and $\eta = 1$.

ization beats [32]. The amplitude fluctuation of the light field is also crucial in the Raman-enhanced polarization beats. On the other hand, because of $\langle u_i(t)\rangle = 0$ and $\langle u_i^*(t)\rangle = 0$, the absolute square of the stochastic average of the polarization $|\langle P^{(3)}\rangle|^2$, which involves second-order coherence function of $u_i(t)$, cannot be used to describe the temporal behavior of the HOCPB [17,25,26]. The second-order coherence function theory is valid when we are only interested in the τ-dependent part of the beating signal. Therefore, the sixth-order coherence function theory is of vital importance in HOCPB. The application of these results to the HOCPB experiment yielded a better fit to the data than an expression involving only second-order coherence. We present experi-

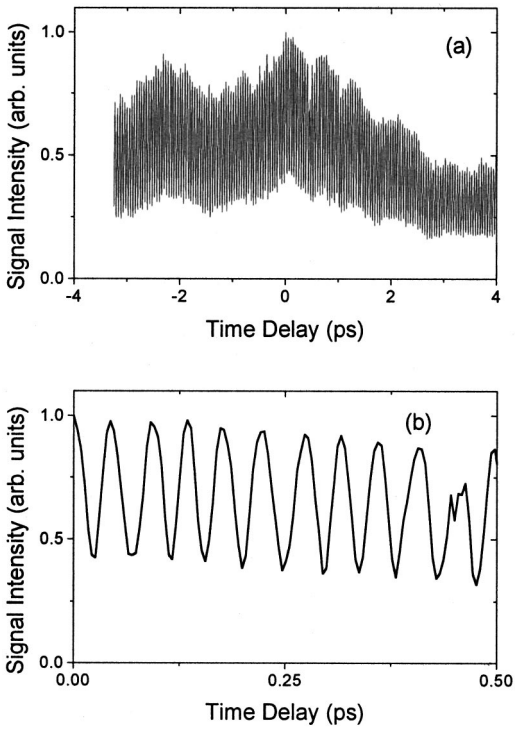

FIG. 9. Experimental result of the beat signal intensity versus relative time delay. (a) Time delay τ is varied for a range of 7.3 ps, (b) Time delay τ is varied for a range of 0.5 ps.

mental results for the material response in cascade-level polarization beats with phase-conjugation geometry using chaotic fields. Beams *A* and *B* are identical in makeup. Each is composed of the same two noisy fields centered at two different colors, ω_1 and ω_2, and carrying its own statistical factors, $u_1(t)$ and $u_2(t)$. Beams *A* and *B* differ only in their wave vector, polarization vector, and time delay. At present, it is difficult to achieve the polarization beat experiment by the phase-diffusion field or the Gaussian-amplitude field. Therefore, it is more difficult to get a clear picture of physical origins of the effects in each type of fluctuating field in the experiment.

V. EXPERIMENT AND RESULT

We perform the HOCPB for a sodium vapor, where the ground state $3S_{1/2}$, the intermediate state $3P_{3/2}$, and excited state $5S_{1/2}$ form a three-level system. Two dye lasers (DL1, and DL2) pumped by the second harmonic of a Quanta-Ray yttrium-aluminum-garnet (YAG) laser, are used to generate frequencies at ω_1 and ω_2. DL1 and DL2 have a linewidth 0.01 nm and a pulse width 10 ns. The values for the relevant transverse relaxation rate for the sodium vapor are 0.175 and 0.085 ps^{-1} [33]. This is narrowband limit. DL1 is tuned to 589 nm, the wavelength of the $3S_{1/2}$-$3P_{3/2}$ transition. DL2 is tuned to 616 nm, the wavelength of the $3P_{3/2}$-$5S_{1/2}$ transition. A beam splitter is used to combine the ω_1 and ω_2 components derived from DL1 and DL2, respectively, for beams *A* and *B*, which intersect in the oven containing the Na vapor. The relative time delay τ between beams *A* and *B* can be varied. Beam 3, which propagates along the direction opposite to that of beam *A*, is derived from DL1. All the incident beams are linearly polarized in the same direction. The beat signal has the same polarization as the incident beams and propagates along a direction almost opposite to that of beam *B*. It is detected by a photodiode.

We first perform a DFWM experiment with beams *A* and *B*, both consisted of only ω_1 frequency component. Figure 5 presents the spectrum of the DFWM. From the DFWM spectrum we tune ω_1 to the resonant frequency Ω_1, whose center wavelength is 589 nm. The center dip of the DFWM spectrum reflects the saturation behaviors of the chaotic field. The relation of the DFWM signal intensity versus relative time delay is showed in Fig. 6. We then perform a NDFWM experiment in which beams *A* and *B* consist of only a ω_2 frequency component, and we measure the NDFWM spectrum by scanning ω_2 (Fig. 7), which shows a resonant profile due to two-photon transition. From the NDFWM spectrum we tune ω_2 to the resonant frequency Ω_2, whose center wavelength is 616 nm. The relation of the NDFWM signal intensity versus relative time delay is shown in Fig. 8. After that, we perform the HOCPB experiment by measuring the beat signal intensity as a function of the relative time delay when beams *A* and *B* consist of both frequencies ω_1 and ω_2. Figure 9 presents experimental result of the beat signal intensity versus relative time delay. The signal modulates sinusoidally with period 45 fs. The modulation frequency can be obtained more directly by making a Fourier transformation of the HOCPB data. Figure 10 shows the Fourier spectrum of the data in which τ is varied for a range of 7.3 ps. Then we obtain the modulation frequency 1.4×10^{14} s^{-1} corresponding to the beating between the resonant frequencies of the transitions from $3S_{1/2}$ to $3P_{3/2}$ and from $3P_{3/2}$ to $5S_{1/2}$.

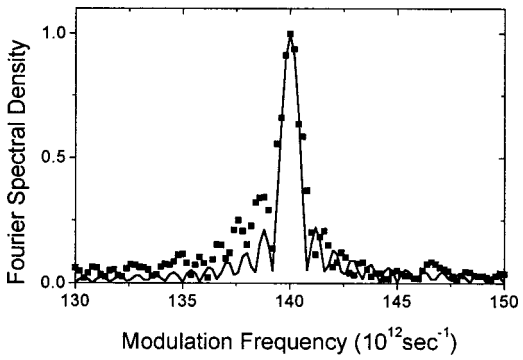

FIG. 10. The square is Fourier spectrum of the experimental data in which τ is varied for a range of 7.3 ps. The solid curve is the theoretical curve given by Eq. (12) with $\alpha_1=2.7\times10^{10}$ s^{-1}, $\alpha_2=2.9\times10^{10}$ s^{-1}, $\omega_2-\omega_1=1.4\times10^{14}$ s^{-1}, $\Delta k=0$, and $\eta=B_i=1$.

Now, we discuss the difference between HOCPB and UMS [24] with self-diffraction geometry from a physical viewpoint. The frequencies and wave vectors of the UMS signal are $\omega_{s_1}=2\omega_1-\omega_1$, $\omega_{s_2}=2\omega_2-\omega_2$, and $\vec{k}_{s_1}=2\vec{k}_1'-\vec{k}_1$, $\vec{k}_{s_2}=2\vec{k}_2'-\vec{k}_2$, respectively, which means that a photon is absorbed from each of the two mutually correlated pump beams. On the other hand, the frequencies and wave vectors of the HOCPB signal are $\omega_{s_1}=\omega_1-\omega_1+\omega_3$, $\omega_{s_2}=\omega_2-\omega_2+\omega_3$, and $\vec{k}_{s_1}=\vec{k}_1-\vec{k}_1'+\vec{k}_3$, $\vec{k}_{s_2}=\vec{k}_2-\vec{k}_2'+\vec{k}_3$, respectively, therefore photons are absorbed from and emitted to the mutually correlated beams *A* and *B*, respectively. This difference between HOCPB and UMS has profound influence on the field-correlation effects. We note that the role of beams *A* and *B* are interchangeable in the UMS, this interchangeable feature also makes the second-order coherence function theory fail in the UMS. Because $\langle u(t_1)u(t_2)\rangle=0$, the absolute square of the stochastic average of the polarization $|\langle P^{(3)}\rangle|^2$ cannot be used to describe the temporal behavior of the UMS [17,25,26]. Our sixth-order theory is of vital importance in the UMS.

In conclusion, we have adopted chaotic, phase-diffusion and Gaussian-amplitude field models to study the effects of sixth-order coherence on polarization beats in a cascade three-level system. The polarization beat signal is shown to be particularly sensitive to the field statistics. Different stochastic models of the laser field only affect the sixth- and fourth-order coherence functions. The constant background of the beat signal originates from the amplitude fluctuation of the Markovian stochastic fields. The Gaussian-amplitude field shows fluctuations larger than the chaotic field, which again exhibits fluctuations much larger than for the phase-diffusion field with pure phase fluctuations caused by spontaneous emission. We have considered the cases that pump beams have either narrow band or broadband linewidth and found that for both cases a Doppler-free precision in the measurement of the energy-level difference of the excited

states can be achieved. It is worth mentioning that the asymmetric behaviors of the polarization beat signals due to the unbalanced dispersion effects of the optical components between the two arms of the interferometer, do not affect the overall accuracy in the case using HOCPB to measure the energy-level difference [9,10,17].

ACKNOWLEDGMENTS

This work was supported by the Chinese National Nature Sciences Foundation (Grant No. 69978019) and the State Key Laboratory Foundation of Transient Optics Technology (Grant No. YAK20006).

[1] R. E. Ryan and T. H. Bergeman, Phys. Rev. A **43**, 6142 (1991).
[2] C. Chen, D. S. Elliott, and M. W. Hamilton, Phys. Rev. Lett. **68**, 3531 (1992).
[3] R. Walser, H. Ritsch, P. Zoller, and J. Cooper, Phys. Rev. A **45**, 468 (1992).
[4] M. H. Anderson, G. Vemuri, J. Cooper, P. Zoller, and S. J. Smith, Phys. Rev. A **47**, 3202 (1993).
[5] R. E. Ryan, L. A. Westling, R. Blumel, and H. J. Metcalf, Phys. Rev. A **52**, 3157 (1995).
[6] A. T. Georges, Phys. Rev. A **21**, 6 (1980).
[7] R. Bratfalean and P. Ewart, Phys. Rev. A **56**, 2267 (1997).
[8] D. J. Ulness and A. C. Albrecht, Phys. Rev. A **53**, 1081 (1996).
[9] D. J. Ulness and A. C. Albrecht, J. Raman Spectrosc. **28**, 571 (1997).
[10] D. C. DeMott, D. J. Ulness, and A. C. Albrecht, Phys. Rev. A **55**, 761 (1997).
[11] D. J. Ulness, J. C. Kirkwood, and A. C. Albrecht, J. Chem. Phys. **108**, 3897 (1998).
[12] J. C. Kirkwood, A. C. Albrecht, D. J. Ulness, and M. J. Stimson, Phys. Rev. A **58**, 4910 (1998).
[13] J. C. Kirkwood, A. C. Albrecht, and D. J. Ulness, J. Chem. Phys. **111**, 253 (1999).
[14] J. C. Kirkwood and A. C. Albrecht, Phys. Rev. A **61**, 033802 (2000).
[15] H. Ma and Cid B. de Araujo, Phys. Rev. Lett. **71**, 3649 (1993).
[16] H. Ma, L. H. Acioli, A. S. L. Gomes, and Cid B. de Araujo, Opt. Lett. **16**, 630 (1991).
[17] Y. P. Zhang, L. Q. Sun, T. T. Tang, and P. M. Fu, Phys. Rev. A **61**, 053819 (2000).
[18] Y. P. Zhang, T. T. Tang, S. Li, and L. Q. Sun, Acta Phys. Sin. **48**, 1452 (1999).
[19] Y. P. Zhang, L. Q. Sun, T. T. Tang, and P. M. Fu, J. Opt. Soc. Am. B **17**, 690 (2000).
[20] Y. P. Zhang, T. T. Tang, L. Q. Sun, and P. M. Fu, Phys. Rev. A **61**, 023809 (2000).
[21] Y. P. Zhang, C. L. Gan, J. P. Zhu, T. T. Tang, and P. M. Fu, Acta Phys. Sin. **48**, 1667 (1999).
[22] Y. P. Zhang, L. Q. Sun, T. T. Tang, L. Zhang, and P. M. Fu, Chin. Phys. Lett. **17**, 206 (2000).
[23] Y. P. Zhang, T. T. Tang, and P. M. Fu, Acta Phys. Sin. **48**, 242 (1999).
[24] D. DeBeer, L. G. Van Wagenen, R. Beach, and S. R. Hartmann, Phys. Rev. Lett. **56**, 1128 (1986).
[25] P. M. Fu, X. Mi, Z. H. Yu, Q. Jiang, Y. P. Zhang, and X. F. Li, Phys. Rev. A **52**, 4867 (1995).
[26] P. M. Fu, Z. H. Yu, X. Mi, X. F. Li, and Q. Jiang, Phys. Rev. A **50**, 698 (1994).
[27] X. Mi, Z. H. Yu, Q. Jiang, Z. G. Zhang, and P. M. Fu, J. Opt. Soc. Am. B **10**, 725 (1993).
[28] N. Morita and T. Yajima, Phys. Rev. A **30**, 2525 (1984).
[29] S. Asaka, M. Nakatsuka, M. Fujiwara, and M. Matsuoka, Phys. Rev. A **29**, 2286 (1984).
[30] V. Kozich, L. D. Menezes, and Cid B. de Araujo, J. Opt. Soc. Am. B **17**, 973 (2000).
[31] R. Trebino, E. K. Gustafson, and A. E. Siegman, J. Opt. Soc. Am. B **3**, 1295 (1986).
[32] Y. P. Zhang, X. Hou, K. Q. Lu, and H. C. Wu, Opt. Commun. **184**, 265 (2000).
[33] J. E. Golub and T. W. Mossberg, J. Opt. Soc. Am. B **3**, 554 (1986).